Supplymentary Material

Tetraphenylethylene-Substituted Bis(thienyl)imidazole (DTITPE), An Efficient Molecular Sensor for the Detection and Quantification of Fluoride Ions

Ranjith Kumar Jakku [1,2,3], Nedaossadat Mirzadeh [2,3], Steven H. Privér [3], Govind Reddy [3,4], Anil Kumar Vardhaman [4], Giribabu Lingamallu [2,4,5], Rajiv Trivedi [1,2,5] and Suresh Kumar Bhargava [2,3,*]

[1] Catalysis and Fine Chemicals Division, CSIR-Indian Institute of Chemical Technology, Uppal Road,
Tarnaka, Hyderabad 500007, India; ranjithkumar4chem@gmail.com (R.K.J.); trivedi@csiriict.in (R.T.)
[2] IICT-RMIT Centre, CSIR-Indian Institute of Chemical Technology, Uppal Road, Tarnaka, Hyderabad 500007, India; nedaossadatmirzadeh@gmail.com (N.M.); giribabu@iict.res.in (G.L.)
[3] Centre for Advanced Materials and Industrial Chemistry (CAMIC), School of Science, RMIT University, GPO Box 2476, Melbourne 3001, Australia; steven.priver@rmit.edu.au (S.H.P.); r.govindreddy@gmail.com (G.R.)
[4] Polymer and Functional Materials Division, CSIR-Indian Institute of Chemical Technology, Uppal Road, Tarnaka, Hyderabad 500007, India; anil1hnk@gmail.com
[5] Academy of Scientific and Innovative Research, AcSIR Headquarters, CSIR-HRDC campus Sector 19,
Kamala Nehru Nagar, Ghaziabad, Uttar Pradesh 201002, India
* Correspondence: suresh.bhargava@rmit.edu.au; Tel.: +61-3-9925-2330

1. Spectroscopy study

1.1 ^{1}H and ^{13}C NMR and mass spectra

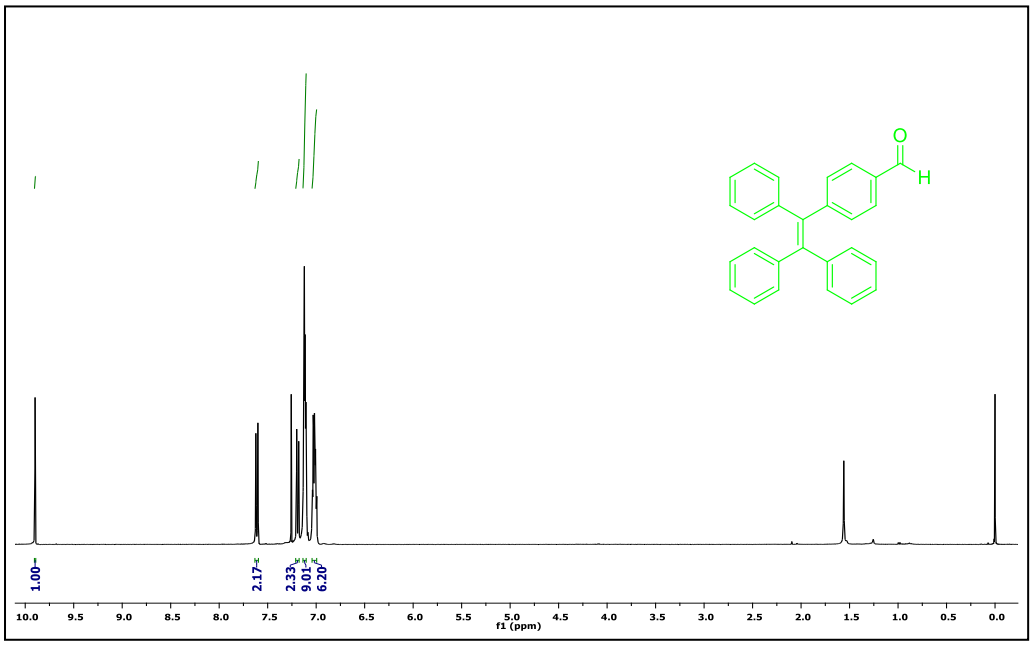

Figure S1. ^{1}H NMR spectrum of 4-(1,2,2-triphenylvinyl) benzaldehyde (400 MHz, $CDCl_3$): δ 9.90 (s, 1H), 7.62 (d, 2H), 7.21 – 7.18 (m, 2H), 7.12 (dd, *J* = 3.7, 3.2 Hz, 9H), 7.01 (ddt, *J* = 4.7, 2.3, 1.6 Hz, 6H).

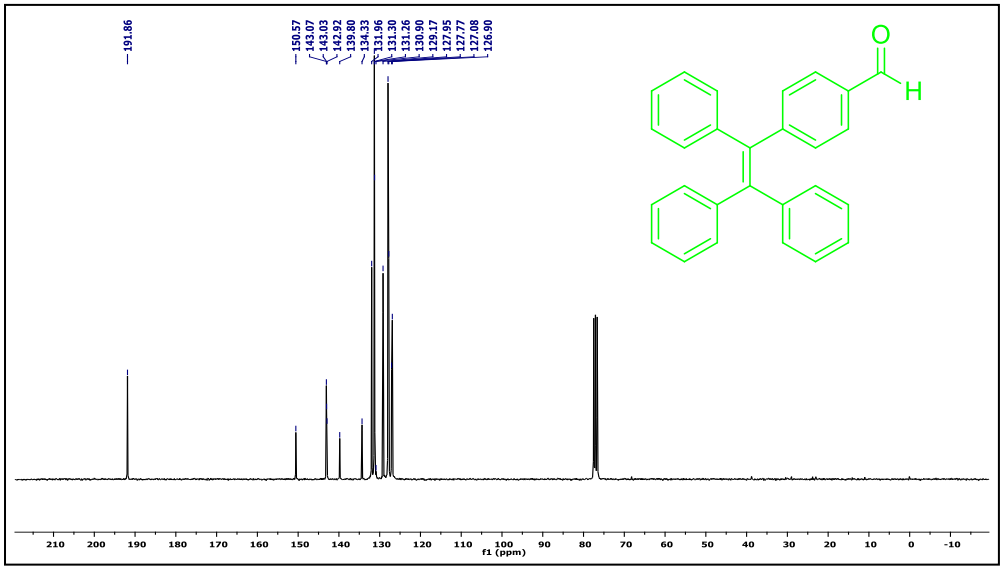

Figure S2. ^{13}C NMR spectrum of 4-(1,2,2-triphenylvinyl) benzaldehyde(75 MHz, $CDCl_3$): δ 191.86, 150.57, 143.07, 143.03, 142.92, 139.80, 134.33, 131.96, 131.30, 131.26, 130.90, 129.17, 127.95, 127.77, 127.08, 126.90.

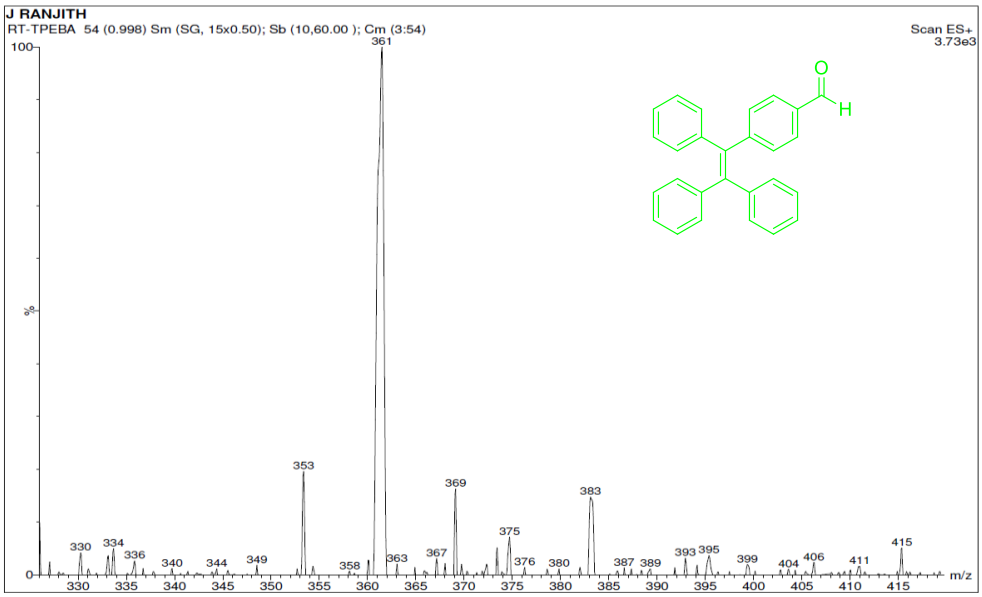

Figure S3. ESI mass spectrum of 4-(1,2,2-triphenylvinyl) benzaldehyde: *m/z* calculated mass for $C_{27}H_{20}O$ m/z=360.1 and found m/z=361 $[M+H]^+$.

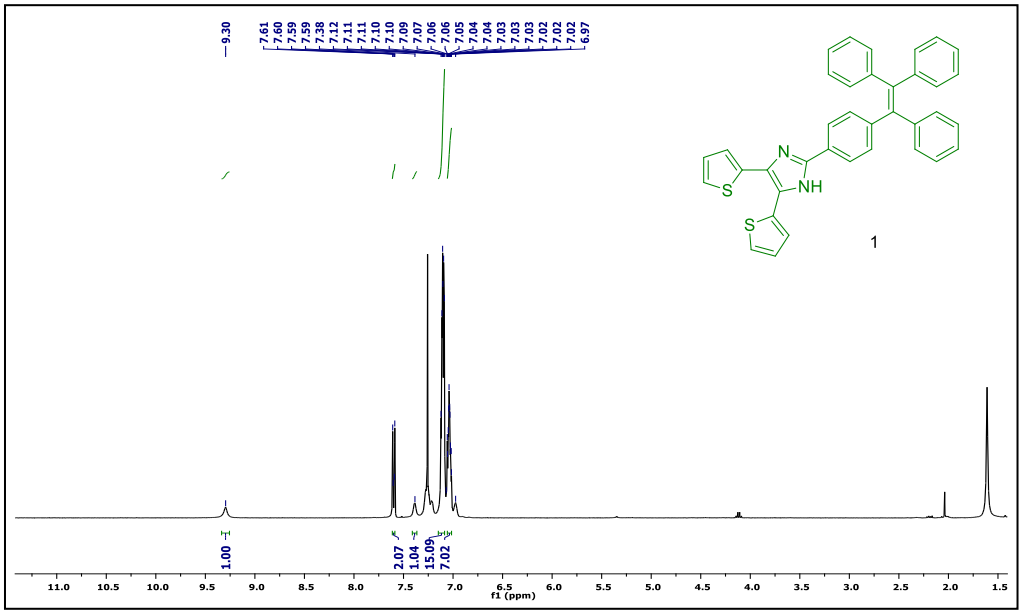

Figure S4. ^1H NMR spectrum of DTITPE (400 MHz, $CDCl_3$) δ 9.30 (s, 1H), 7.61 – 7.59 (m, 2H), 7.38 (s, 1H), 7.10 (td, *J* = 6.1, 3.3 Hz, 15H), 7.06 – 7.02 (m, 7H).

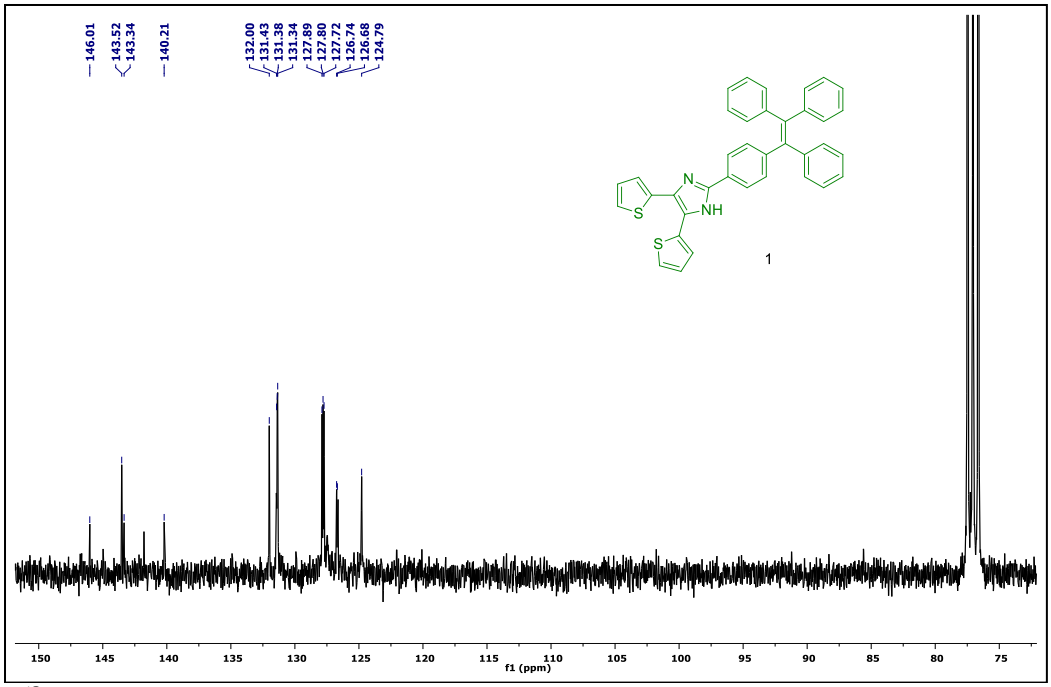

Figure S5. ^{13}C NMR spectrum of DTITPE (75 MHz, $CDCl_3$) δ 146.01, 143.52, 143.34, 140.21, 132.00, 131.43, 131.38, 131.34, 127.89, 127.80, 127.72, 126.74, 126.68, 124.79.

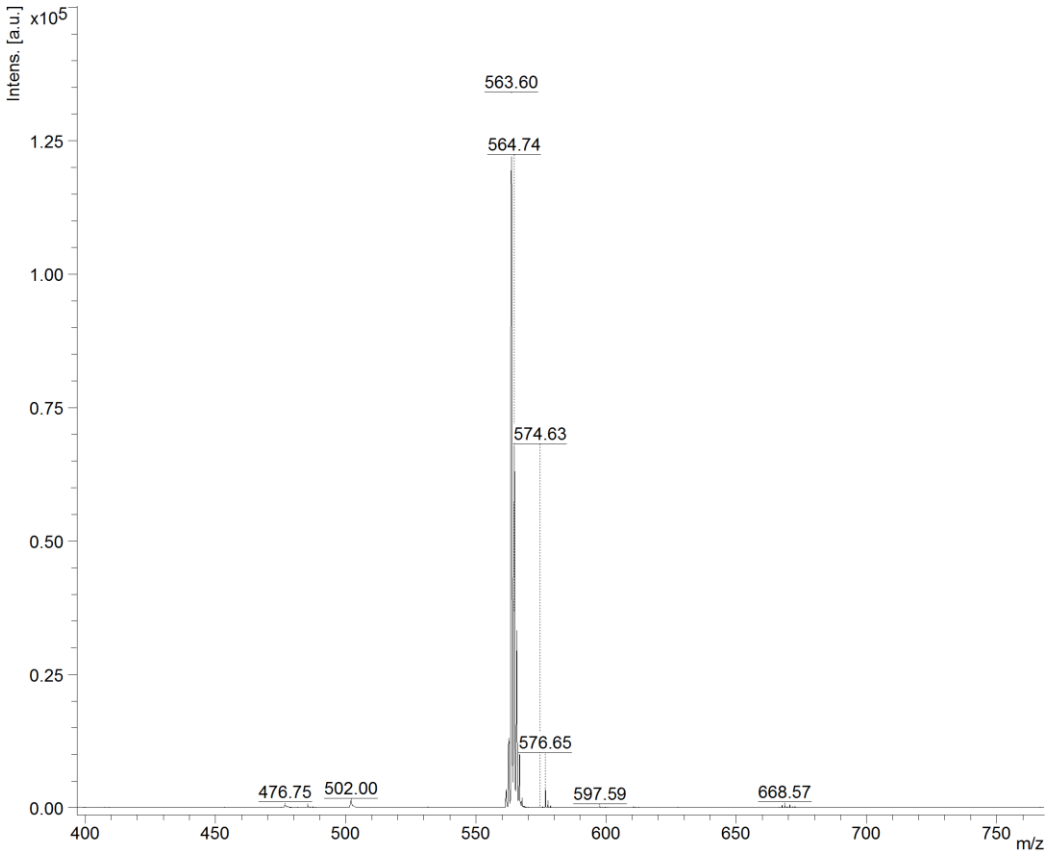

Figure S6. MALDI-TOF mass spectrum for DTITPE: *m/z* calculated for $C_{37}N_{27}S_2$: 563.2; found: 563.6 $[M+H]^+$.

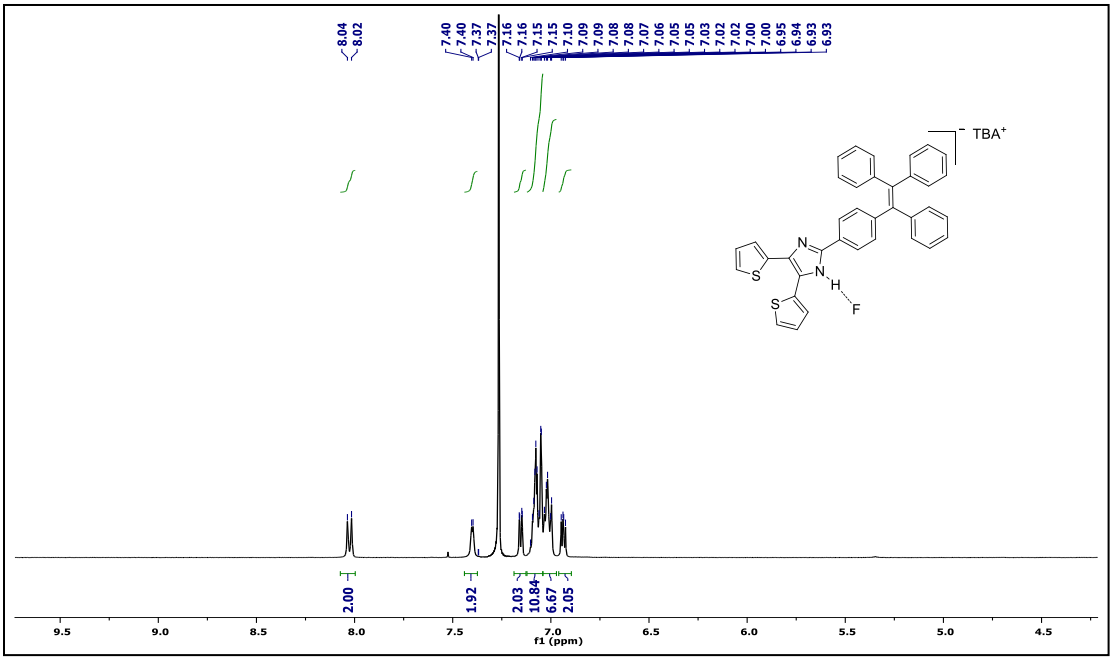

Figure S7. ^{1}H NMR spectrum of DTITPE.F^{-} (400 MHz, $CDCl_3$): δ 8.03 (d, *J* = 8.4 Hz, 2H), 7.40 (d, *J* = 2.9 Hz, 2H), 7.15 (dd, *J* = 5.1, 0.9 Hz, 2H), 7.12 – 7.04 (m, 10H), 7.04 – 6.97 (m, 6H), 6.94 (dd, *J* = 5.0, 3.6 Hz, 2H).

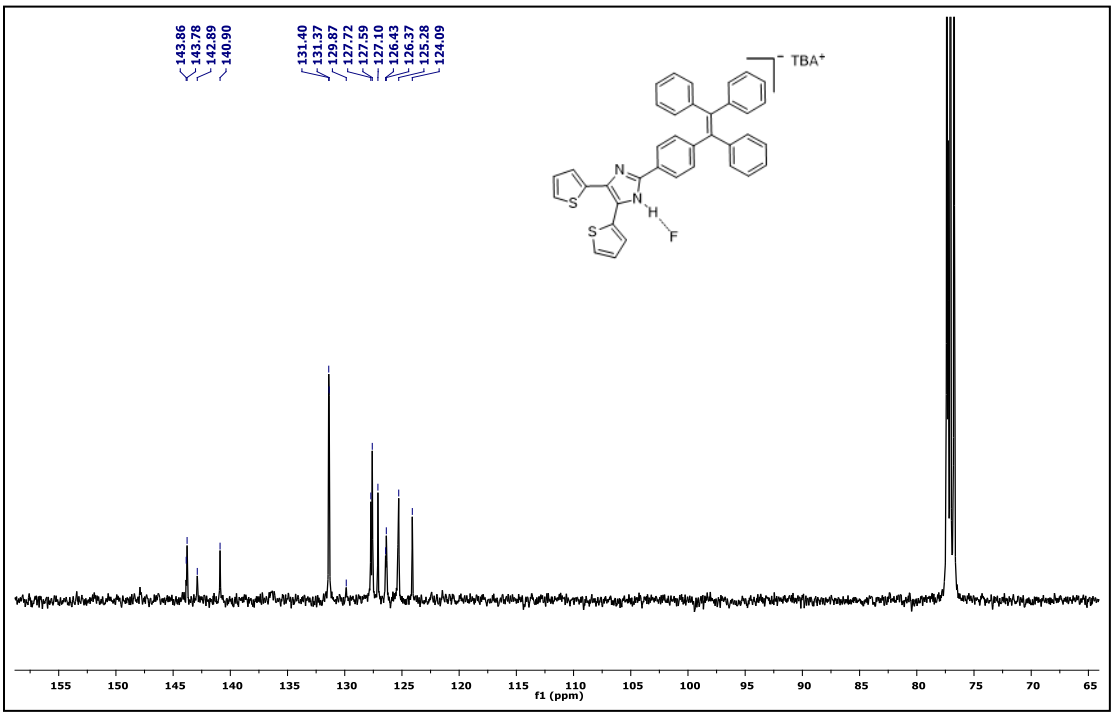

Figure S8. ^{13}C NMR spectrum of DTITPE.F^{-} (101 MHz, $CDCl_3$): δ 143.86, 143.78, 142.89, 140.90, 131.40, 131.37, 129.87, 127.72, 127.59, 127.10, 126.43, 126.37, 125.28, 124.09.

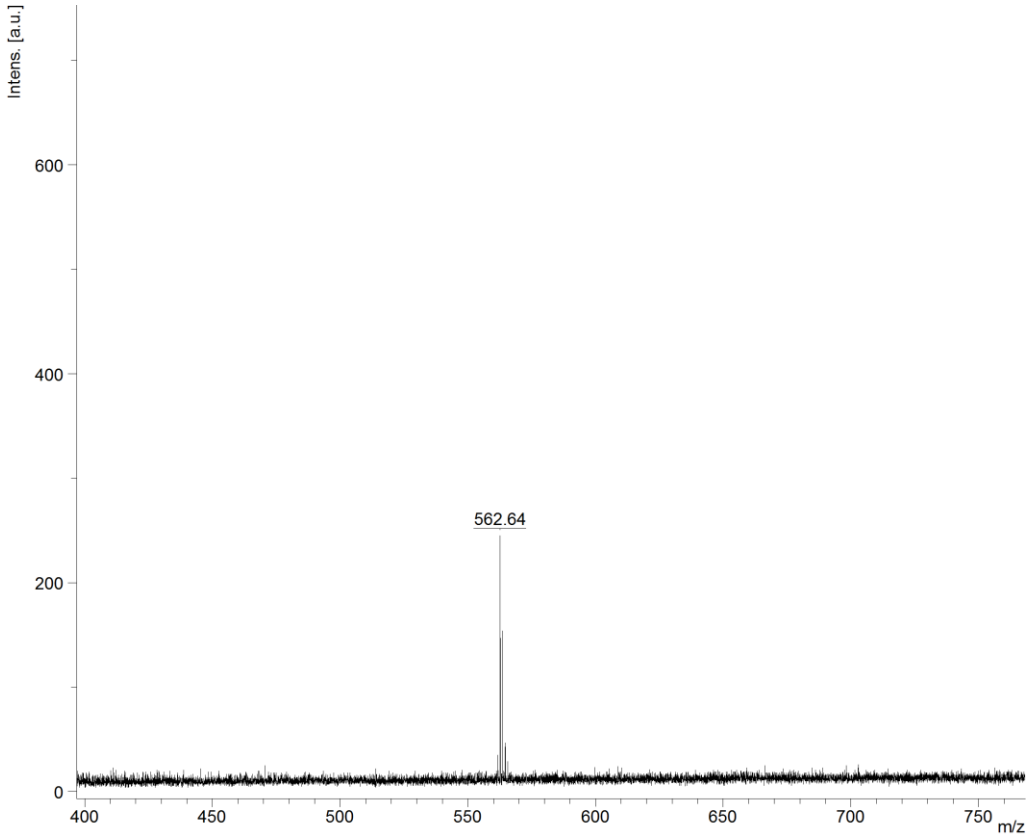

Figure S9. MALDI-TOF mass spectrum for $DTITPE^-$, calculated mass m/z= 561.15 and found m/z=562.5 $[M+H]^+$.

2. FT- IR Spectra

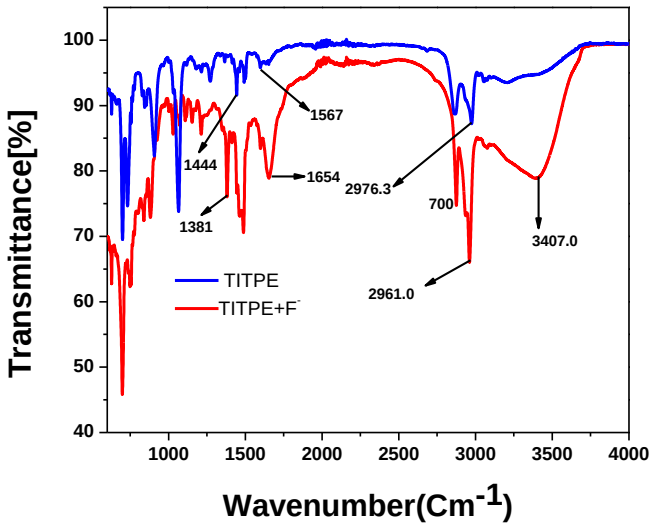

Figure S10. FT-IR spectra of TITPE and $TITPE.F^-$

3. U.V-vis. and Fluorescence data

3.1 Benesi-Hildebrand and LOD plots from UV-Vis. data

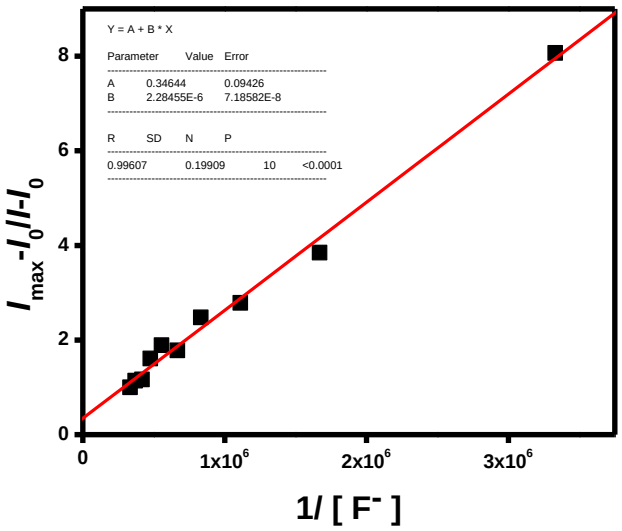

Figure S11. Benesi-Hildebrand plot for the determination of the binding constant of DTITPE in THF using fluorescence emission data.

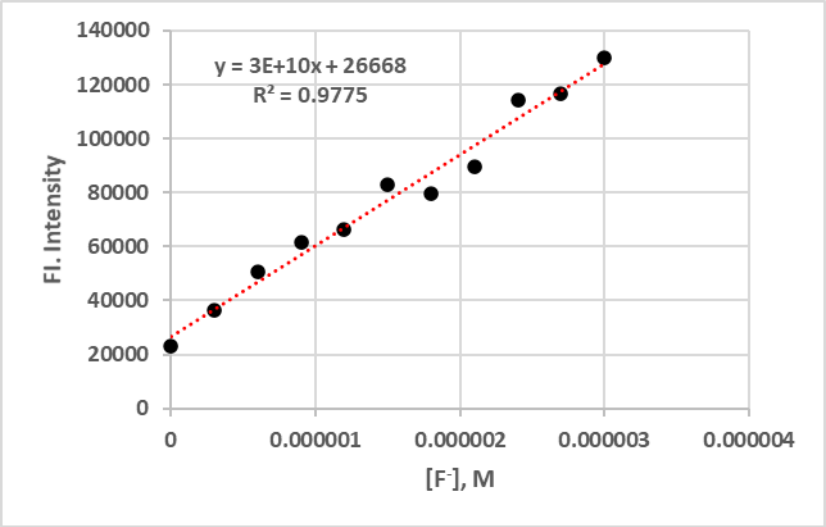

Figure S12. Determination of the detection limit of DTITPE in THF using fluorescence emission data.

3.2 Benesi-Hildebrand and LOD plots from UV-vis. data

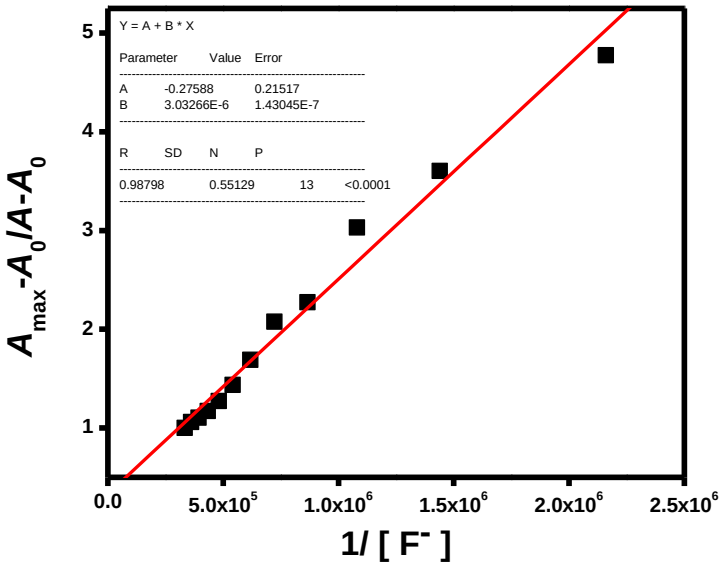

Figure S13. Benesi-Hildebrand plot for the determination of the binding constant of DTITPE in THF using UV-vis. absorption data.

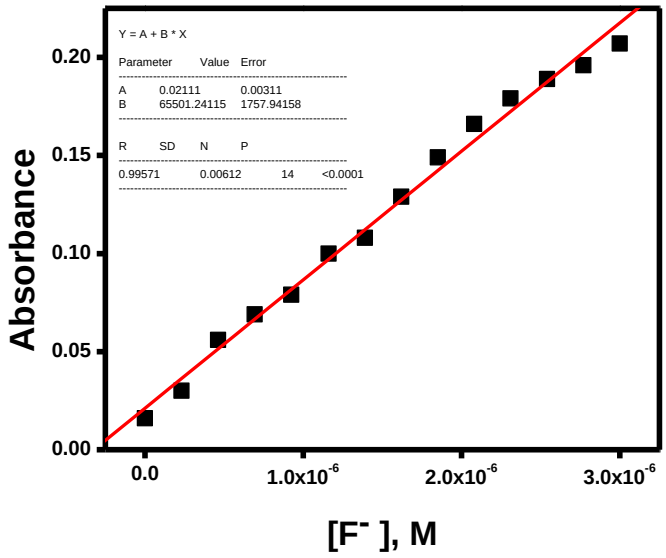

Figure S14. Determination of the detection limit of DTITPE in THF using UV-vis. absorption data in THF.

3.3 Job's plot

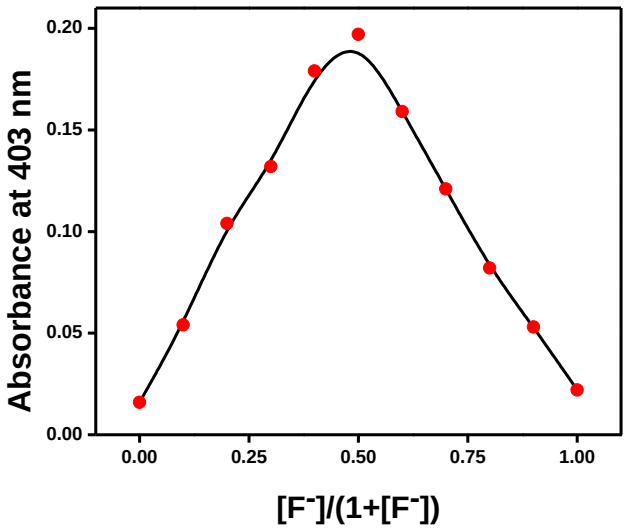

Figure S15. Determination of the stoichiometric ratio between DTITPE and F^- in THF by Job's plot.

3.4 ^{1}H-NMR Data

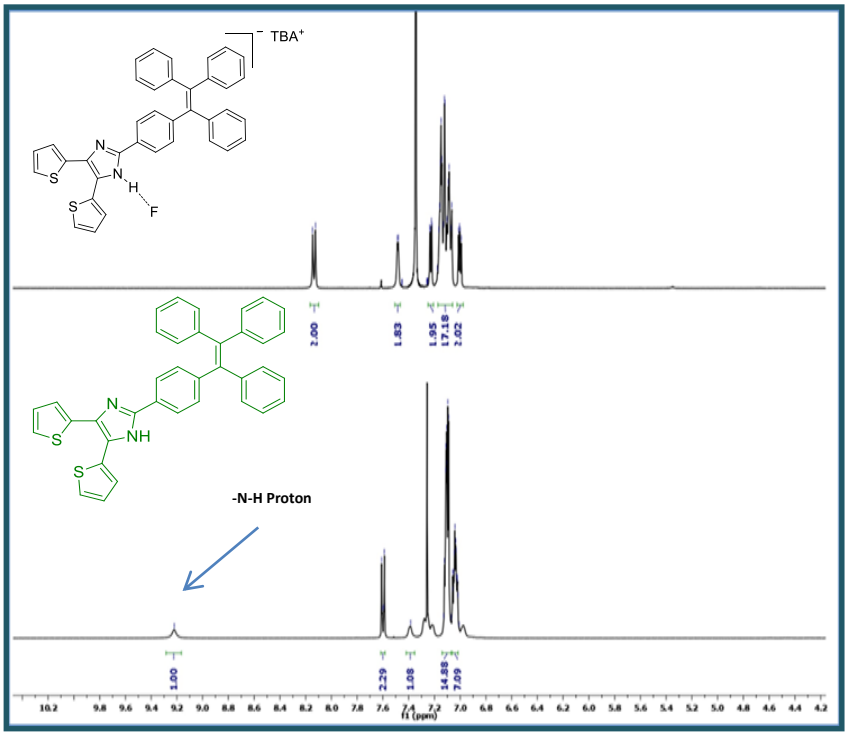

Figure S16a. ^{1}H NMR Spectra of DTITPE and DTITPE.F^-.

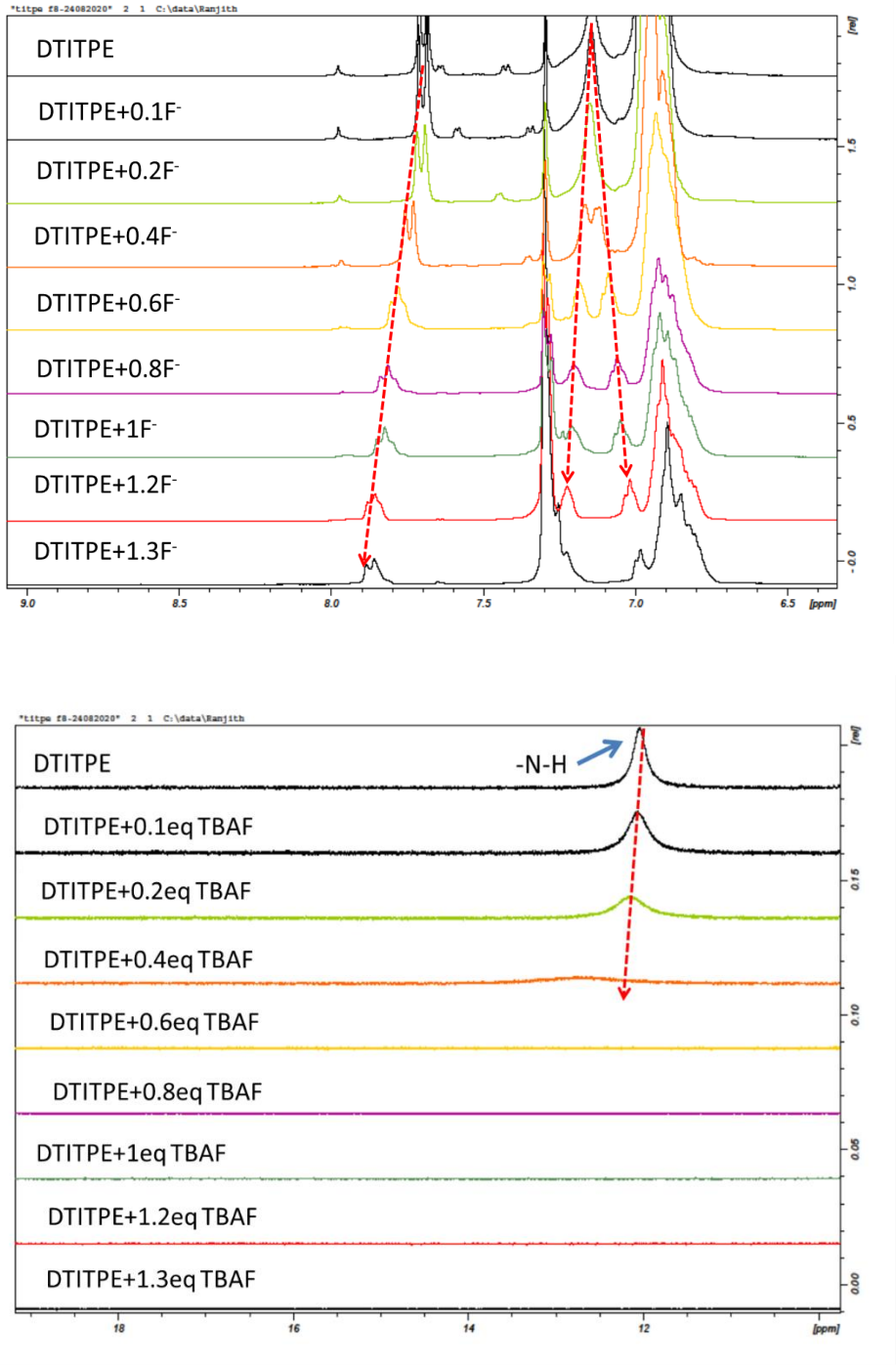

Figure S16b. ^{1}H NMR spectrum of the molecular sensor DTITPE with incremental addition of TBAF, in $CDCl_3$ at room temperature.

4. **DFT Studies**

4.1 Optimized geometry of DTITPE: B3LYP/6-31+G(d,p)

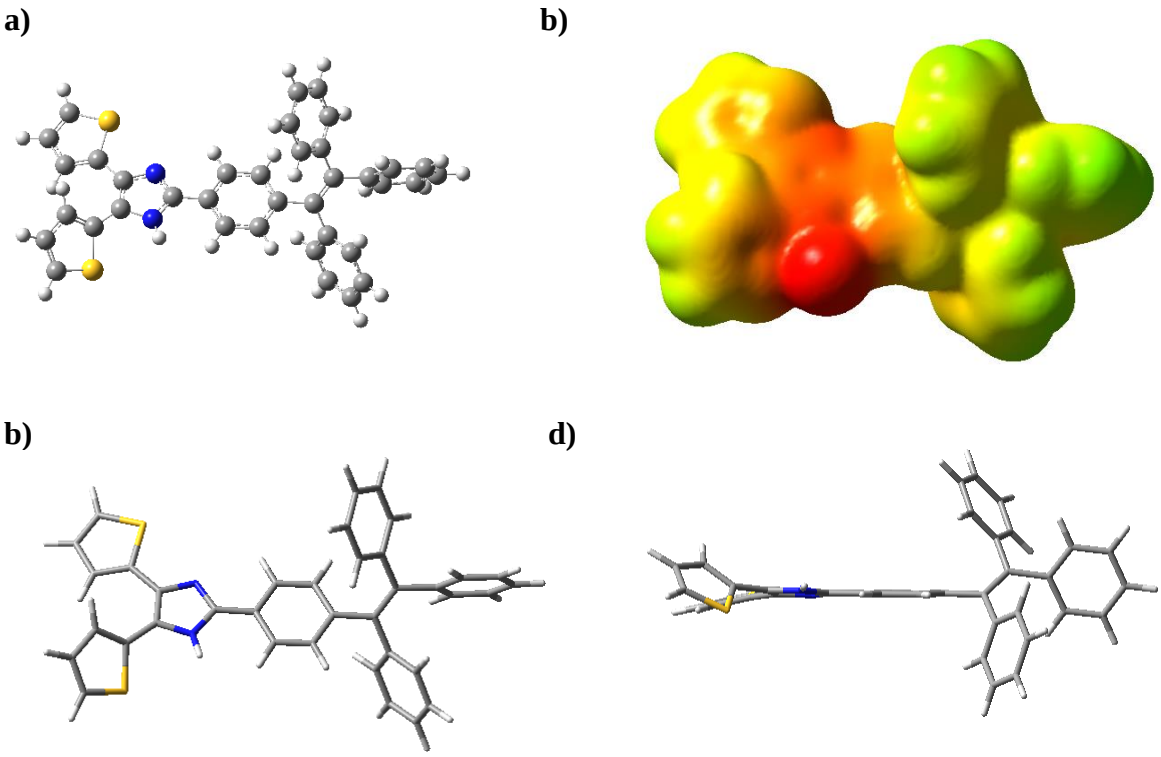

Figure S17: Optimized geometry of DTITPE, b) Electrostatic potential (ESP) (isovalue = 0.02) surfaces of DTITPE, c) Top view of DTITPE, and d) Side view of DTITPE.

From the optimized structure, the N-H distance is 1.009 Å, the dihedral angle between two thiophene rings is -4.48°, dihedral angle between the two *cis* phenyl rings is 11.93°, and the dihedral angle between the two *trans* phenyl rings -167.80°

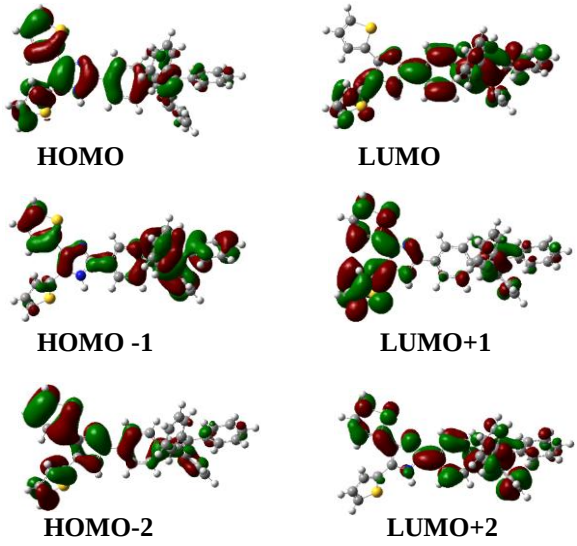

Figure S18. DFT optimized electronic distributions of DTITPE for various HOMO and LUMO energy levels.

4.2 Optimized geometry of DTITPE.F^- with F: B3LYP/6-31+G(d,p)

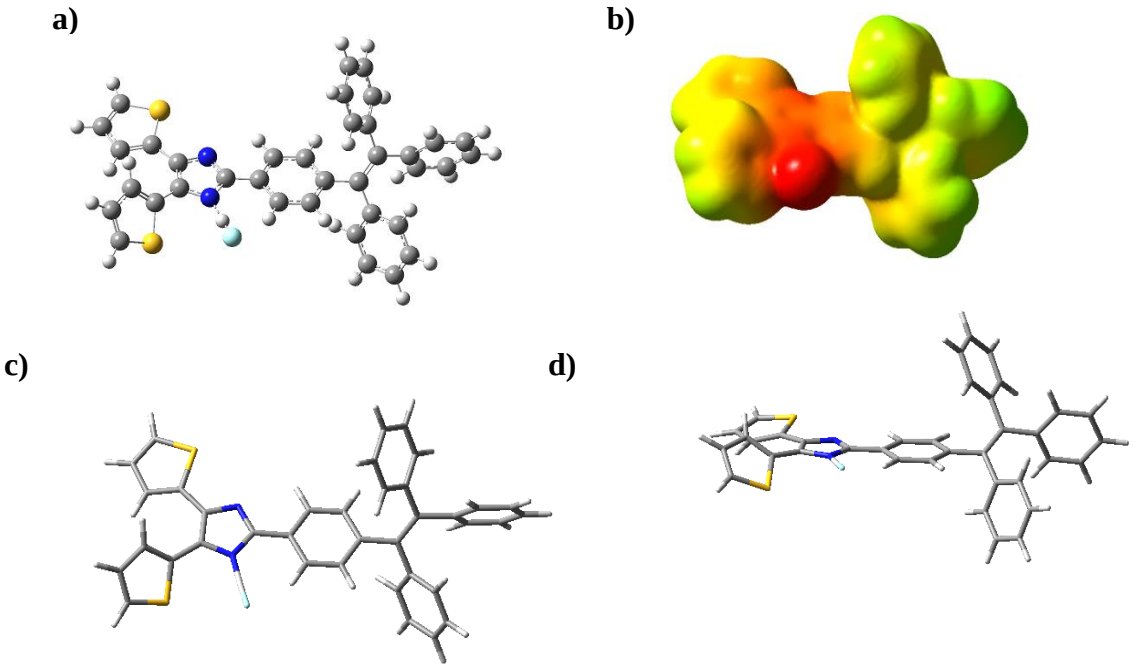

Figure S19 a) Optimized geometry of DTITPE.F^- b) Electrostatic potential (ESP) (isovalue = 0.02) surface of DTITPE.F^- c) Top view of DTITPE.F^-, and d) Side view of DTITPE.F^-

For the geometry optimized structure, the N-H distance is 1.474 Å, the N-H---F^- distance is 1.025 Å, the dihedral angle between two thiophene rings is -4.60°, the dihedral angle between

two *cis* phenyl rings is 13.26°, and the dihedral angle between the two *trans* phenyl rings -166.65°.

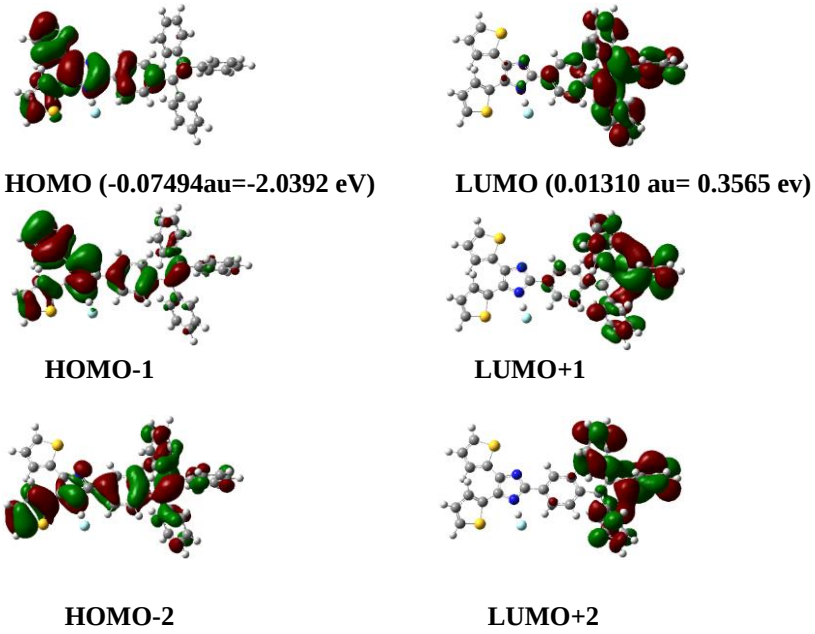

Figure S20. DFT optimized electronic distributions of DTITPE.F^- at various HOMO and LUMO energy levels.

4.3 Optimized geometry of deprotonated DTITPE (DTITPE$^-$): B3LYP/6-31+G(d,p):

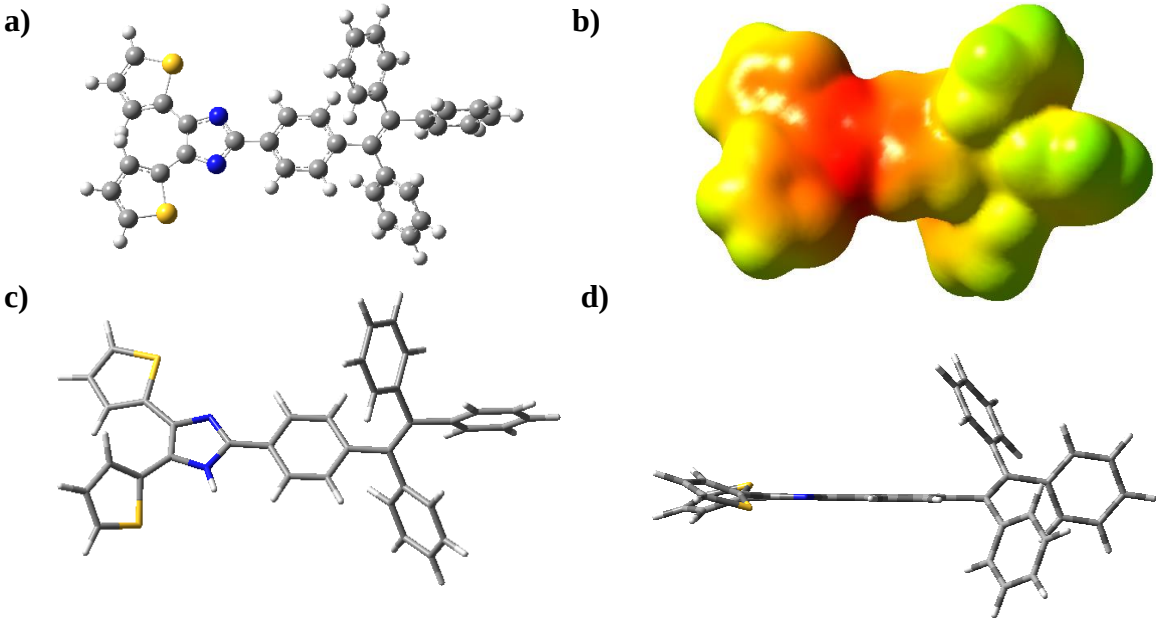

Figure S21 a) Optimized geometry of deprotonated DTITPE$^-$, b) The electrostatic potential (ESP) (isovalue = 0.02) surface of DTITPE$^-$, c) Top view of DTITPE$^-$, and d) Side view of DTITPE$^-$.

From the optimized geometry, the dihedral angle between the two thiophene rings is -5.01°, the dihedral angle between the two *cis* phenyl rings is 14.09°, and the dihedral angle between the two *trans* phenyl rings is -165.79°

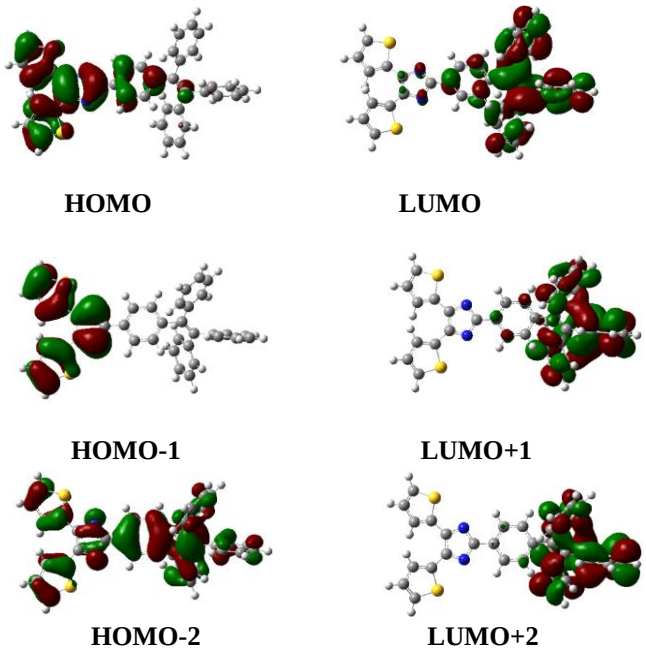

Figure S22. DFT optimized electronic distributions of DTITPE$^-$ at various HOMO and LUMO energy levels.

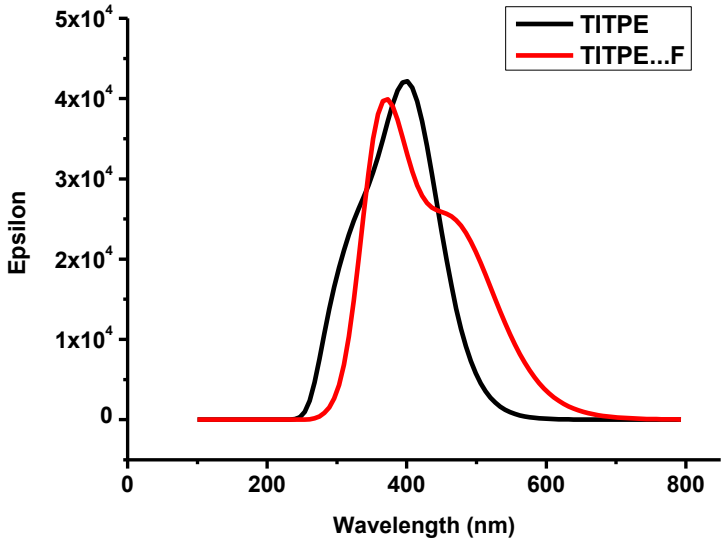

Figure S23: Theoretical UV-vis. spectra for DTITPE and DTITPE.F$^-$ calculated using TD-DFT/B3LYP/6-31+G(d,p) with the CPCM method using THF as solvent**.**

Table S1. Calculated bond lengths and dihedral angles of DTITPE, DTITPE.F$^-$ and DTITPE$^-$ using B3LYP/6-31+G(d,p) method.

	N-H	N-H---F$^-$	**Dihedral angles between two thiophene rings**	**Dihedral angles between two phenyl rings**	
				Cis	***Trans***
DTITPE	1.009 Å	-	-4.48°	11.93°	-167.80°
DTITPE.F$^-$	1.474 Å	1.025 Å	-4.60°	13.26°	-166.65°
DTITPE$^-$	-	-	-5.01°	14.09°	-165.79°

Table S2: Calculated HOMO and LUMO energies and band gaps for DTITPE, DTITPE.F^- and DTITPE$^-$ calculated using B3LYP/6-31+G(d,p) method

HTM	HOMO (eV)	LUMO (eV)	Band gap (eV)	Dipole moment B3lyp/6-31+G(d,p)	Transition dipole Moment B3lyp/6-31+G(d,p)-pcm
DTITPE	-5.247	-1.824	3.423	3.0708	11.6290
DTITPE.F^-	-2.039	0.356	1.683	11.4063	8.4150
DTITPE$^-$	-1.663	0.412	1.250	12.0619	9.1926

Table S3: Theoretical energy levels and MO character for DTITPE, DTITPE.F^- and DTITPE$^-$ calculated using TD-DFT/B3LYP/6-31+G(d,p) with CPCM method using THF as solvent

Compound		λ (nm)	CIC	OS(f)
DTITPE,	S0 to S1	406.70	HOMO->LUMO (98%)	0.8198
DTITPE.F^-	S0 to S1	648.92	H-1->LUMO(55%), HOMO->LUMO (24%)	0.17
	Excited State 7	396.20	H-9->LUMO (22%), H-7->LUMO (13%), H-4->LUMO (38%)	0.03
DTITPE$^-$	Excited State 11	441.61	HOMO->L+1 (67%)	0.16

Table S4: Comparison of the imidazole derived molecular sensors and their sensing properties.

Sensor no	**Mechanism**	**Detection limit (M)**	**Stoichiometry**	**Reference**
1	H-bonding interaction and subsequent deprotonation of imidazole.	$5.63X\ 10^{-5}$	1:2	1
2	H- bonding induced internal charge transfer.	$<0.3X10^{-3}$	1:1	2
3	Formation of hydrogen bonding with imidazole N-H	1.8×10^{-6}	1:2	3
4	Deprotonation of imidazole N-H.	0.5×10^{-6}	1:1	4
5	Formation of hydrogen bonding with imidazole N-H	1.37×10^{-7}	1:1	This work

5 X- ray Crystallographic Data

Crystals of DTITPE suitable for single-crystal X-ray diffraction were obtained from THF/hexane. Using a drop of inert oil (Paratone), a selected crystal was mounted on a nylon loop and transferred to a stream of cold nitrogen. The reflections were collected on a D8 Bruker diffractometer equipped with an APEX-II area detector using graphite-monochromated Mo Kα radiation (λ = 0.71073 Å) from a 1 μS microsource. The computer programs SMART [5] and SAINT [6] were used for data collection and data processing, respectively, and absorption corrections using SADABS [7]. The structure was solved using direct methods and refined with full-matrix least-squares methods on F_2 using the SHELXTL package [8-9]. The imidazole proton was located in the difference Fourier map and the thienyl group containing S1 was disordered (0.749:0.251) by a 180° rotation about the C28–C30 bond. The CCDC number for DTITPE is 1988020

Table S5. Crystal data and structure refinement for DTITPE.

Identification code	TITPE
Empirical formula	C37 H26 N2 S2
Moiety formula	C37 H26 N2 S2
Formula weight	562.72
Temperature	100(2) K
Wavelength	0.71073 Å
Crystal system	Orthorhombic
Space group	Pn a 21
Unit cell dimensions	
α= 90°	a = 9.1492(15) Å
β= 90°	b = 21.940(4) Å
γ = 90°	c = 14.903(3) Å
Volume	2991.7(9) Å3
Z	4
Density (calculated)	1.249 Mg/m3
Absorption coefficient	0.207 mm^{-1}
F(000)	1176
Crystal size	0.482 x 0.134 x 0.094 mm^3
Theta range for data collection	1.652 to 29.940°
Index ranges	-11<=h<=12, -30<=k<=27, -20<=l<=20
Reflections collected	32612
Independent reflections	8620 [R(int) = 0.0288]
Observed reflections	7933
Completeness to theta = 29.940°	99.9 %
Absorption correction	Semi-empirical from equivalents
Max. and min. transmission	0.746 and 0.723
Refinement method	Full-matrix least-squares on F2

Data / restraints / parameters	8620 / 6 / 386
Goodness-of-fit on F2	1.032
Final R indices [I>2sigma(I)]	R1 = 0.0356, wR2 = 0.0880
R indices (all data)	R1 = 0.0407, wR2 = 0.0910
Absolute structure parameter	0.095(19)
Extinction coefficient	n/a
Largest diff. peak and hole	0.478 and -0.312 e.Å-3

References

1. Wu, Y.-C.; Huo, J.-P.; Cao, L.; Ding, S.; Wang, L.-Y.; Cao, D.; Wang, Z.-Y., Design and application of tri-benzimidazolyl star-shape molecules as fluorescent chemosensors for the fast-response detection of fluoride ion. *Sens. Actuators B Chem.* **2016,** *237*, 865-875, doi: 10.1016/j.snb.2016.07.028
2. Swami, S.; Behera, D.; Agarwala, A.; Verma, V. P.; Shrivastava, R., β-Carboline–imidazopyridine hybrids: selective and sensitive optical sensors for copper and fluoride ions. *New J. Chem.* **2018**, 42, 10317-10326, doi: 10.1039/c8nj01851k
3. Naha, S.; Velmathi, S. J. C., Phenazine‐Based Fluorescence "Turn‐Off" Sensor for Fluoride: Application on Real Samples and to Cell and Zebrafish Imaging. *ChemistrySelect*, **2019,** 4, 2912-2917, doi: 10.1002/slct.201803702
4. Bhattacharyya, B.; Kundu, A.; Guchhait, N.; Dhara, K. J. J. o. f., Anthraimidazoledione Based Reversible and Reusable Selective Chemosensors for Fluoride Ion: Naked-Eye, Colorimetric and Fluorescence "ON-OFF". *J. Fluoresc.* **2017,** 27, 1041-1049, doi:10.1007/s10895-017-2038-x.
5. SMART Software ver. 5.625 for the CCD Detector System; Bruker AXS Inc.: Madison, WI, USA, 2001.
6. SAINTPLUS software ver. 6.22 for the CCD Detector System; Bruker AXS Inc.: Madison, WI, USA, 2001.
7. Blessing, R.H. An empirical correction for absorption anisotropy. *Acta Crystallogr., Sect. A: Found. Crystallogr.* **1995**, 51, 33–38, doi.org/10.1107/S0108767394005726.
8. Sheldrick, G.M. SHELXTL software ver. **2013/4**; Universität Göttingen: Göttingen, Germany, 2013.
9. Sheldrick, G.M. A short history of SHELX. *Acta Crystallogr., Sect. A: Found. Crystallogr.* **2008**, 64, 112–122, doi.org/10.1107/S0108767307043930